AMERICAN SCIENTIFIC PUBLISHERS

Science of Advanced Materials
Vol. 6, pp. 1–10, 2014
(www.aspbs.com/sam)

ARTICLE

Comparative Raman Study of Organic-Free and Surfactant-Capped Rod-Shaped Anatase TiO_2 Nanocrystals

Barbara Federica Scremin[1,*], Maria R. Belviso[1], Davide Altamura[2], Cinzia Giannini[2], and P. Davide Cozzoli[1,3,*]

[1]*National Nanotechnology Laboratory (NNL)-CNR Istituto Nanoscienze, c/o Distretto Tecnologico, via per Arnesano km 5, I-73100 Lecce, Italy*
[2]*Istituto di Cristallografia (IC)-CNR, via Amendola 122/O, I-70126 Bari, Italy*
[3]*Dipartimento di Matematica e Fisica "E. De Giorgi," Università del Salento, via per Arnesano, I-73100 Lecce, Italy*

ABSTRACT

Excitation of lattice vibrations in nanostructured anatase TiO_2 frequently occurs at energy values differing from that found for the corresponding bulk phase. Particularly, investigations have long aimed at establishing a correlation between the low-frequency $E_g(1)$ mode and the mean crystallite size on the basis of phonon-confinement models. Here, we report a detailed Raman study, supported by X-ray diffraction analyses, on anatase TiO_2 nanocrystals with rod-shaped morphology and variable geometric parameters, prepared by colloidal wet-chemical routes. By examining the anomalous shifts of the $E_g(1)$ mode in the spectra of surfactant-capped nanorods and in those of corresponding organic-free derivatives (obtained by a suitable thermal oxidative treatment), an insight into the impact of exposed facets and of the coherent crystalline domain size on Raman-active lattice vibrational modes has been gained. Our investigation offers a ground for clarifying the current lack of consensus as to the applicability of phonon-confinement models for drawing information on the size of surface-functionalized TiO_2 nanocrystals upon analysis of their Raman features.

KEYWORDS: TiO_2, Colloidal Nanocrystals, Raman Spectroscopy, X-Ray Diffraction.

1. INTRODUCTION

TiO_2 nanomaterials, particularly in the tetragonal anatase phase, are intensively studied due to their outstanding performance in photocatalysis[1–4] and sunlight energy conversion.[5–7] The controlled synthesis of TiO_2 nanocrystals constitutes an incredibly broad field of experimental research, as crystal structure and geometric parameters indeed dictate their ultimate chemical-physical properties,[8] impacting on their behaviour in processes and devices.[9, 10] The special efforts that have been devoted to tailor TiO_2 in different dimensional and morphological regimes are justified by theoretical predictions and experimental assessment of the size and shape dependence of its chemical reactivity, related to the nature and relative extension of exposed surface facets.[11–13] Recent theoretical studies have predicted the size and shape dependence of the anatase-to-rutile phase transition for TiO_2 crystals to strongly correlate with their surface chemistry features at the nanoscale, explaining the diversity of TiO_2 nanocrystal product achievable in specific synthesis conditions.[14] According to a quantum chemical study,[15] anatase ranks approximately halfway in the size-dependent thermodynamic stability sequence of the most common TiO_2 polymorphs: rutile → brookite → anatase → TiO_2(B) → two-dimensional lepidocrocite. In line with these calculations, the thermodynamic stability order deduced from experimental calorimetric data[16] has been assessed to be: rutile > brookite > anatase (brookite → rutile, $\Delta H° = -0.17 \pm 0.09$ kcal mol^{-1}; anatase → rutile, $\Delta H° = -0.78 \pm 0.20$ kcal mol^{-1}). Taken together, these findings suggest that relatively larger nanocrystals should be expected to preferably take the rutile structure, while medium-size nanocrystals and tiny clusters should be more stable in anatase and lepidocrocite habits, respectively, if their growth is accomplished under close-to-equilibrium conditions.[14, 15]

Raman spectroscopy represents a valuable investigative tool, susceptible to continued refinement, for not only straightforwardly assessing the phase identity of TiO_2 nanomaterials, but also indirectly probing subtle structural deviations associated with crystallite

*Authors to whom correspondence should be addressed.
Emails: barbara.scremin@unisalento.it, davide.cozzoli@unisalento.it
Received: xx Xxxx Xxxx
Accepted: xx Xxxx Xxxx

geometry, stoichiometry, lattice defects, surface status, and strain.[20, 24, 50–52]

Size-related effects have been commonly observed in Raman spectra of nanostructured anatase crystals. Earlier Raman studies evidenced that that the lowest-energy vibrational mode, denoted as $E_g(1)$, which falls at around 144 cm^{-1} for the bulk,[17] lay at variable energies in nanocrystals.[18] The $E_g(1)$ peak was observed to systematically blue-shift with decreasing nanocrystal size, an effect that had initially been thought to be exploitable to extrapolate the particle size in the absence of data from other techniques[19, 20] through evaluating the degree of $E_g(1)$ phonon confinement.[19, 21–23] Yet, it has later been pointed out that the use of Raman scattering data for the characterization of nanocrystal size still requires significant theoretical and experimental advances, before it may be considered as a reliable approach for size determination.[21, 24] Among the reasons limiting utilization of Raman data for such purpose are the lack of knowledge of dispersion relations for anatase (due to unavailability of sufficiently large anatase single crystals[25]), and the fact that current phonon-confinement models do not take into account the size- and shape-dependent effects of lattice dilatation/contraction, stoichiometry deviations, anharmonicity, and local electric field.[21, 26] Finally, it should be recalled that "surface effects," which have frequently been invoked as potentially relevant sources of the unsatisfactory agreement between the size predicted taking into account phonon confinement and that estimated on the basis experimental spectroscopic data, still remain poorly investigated and thus marginally understood. Little experimental evidence is available on the impact of surface-driven compressive stress on Raman vibrational modes.[46] Recently, a stress-modified phonon-confinement model has been proposed by Osterlund et al.[27] in which surface strain was accounted for by pressure fields distributed across the nanocrystals. In another model proposed by Sun et al.[28] the bulk elastic modulus, which exhibits size and shape dependence in nanocrystals, was put in relation with microscopic quantities (such as the characteristics of a selected chemical bond taken as representative of the entire lattice) in a phenomenological way (via a local averaging procedure). To our best knowledge, Raman studies dealing with nanoscale anatase TiO_2 have most exclusively examined nanocrystals with spherical or nearly isotropic shapes, where the different exposed surfaces are approximately equally extended over the particle surface. In contrast, anisotropic nanocrystals are inherently characterized by a largely asymmetric distribution of different facets, depending on the particular morphology and the relative degree of shape anisotropy concerned.

In the present work, we report on a detailed Raman study of anatase TiO_2 nanocrystals with rod-like morphology and variable aspect ratio, prepared by wet-chemical routes. By examining the shift of the low-energy $E_g(1)$ mode in the Raman spectra of surfactant-capped nanorods and those of their corresponding bare (i.e., organic-free) counterparts (obtained by a suitable thermal treatment) with intact crystal phase and comparable geometric features, we have gained insight into the impact of exposed surfaces and of the "effective" crystalline domain size on Raman-active lattice vibrational modes. This investigation offers a basis for clarifying the current lack of consensus as to the applicability of phonon-confinement models for drawing information on the size of surface-functionalized TiO_2 nanoparticles upon analysis of their Raman features.

2. EXPERIMENTAL DETAILS

2.1. Sample Preparation

2.1.1. Nanocrystal Synthesis

Organic-capped TiO_2 anatase nanorods with diameter of about 3–4 nm and lengths adjustable in the 15–50 nm range were synthesized and purified according to well-established colloidal protocols.[29, 30] Three sets of nanorods with variable aspects ratios (i.e., length-to-diameter ratio, AR) of 4, 8, and 16, henceforth referred to as batches AR4, AR8 and AR16, respectively, were prepared. More in detail, AR4 and AR8 were prepared by base-catalysed hydrolysis of titanium tetraisopropoxide in either 1-nanoic acid or oleic acid at 100 °C, respectively.[30] AR16 was prepared by nonaqueous sol–gel condensation of titanium tetraisopropoxide and oleic acid at 270 °C.[29] Nanocrystal size and shape features were inspected by recording low-resolution transmission electron microscopy (TEM) images with a Jeol JEM 1011 microscope operating at 100 kV. Samples for TEM analyses were prepared by dropping a dilute chloroform solution of freshly prepared nanorods onto carbon-coated copper grids and then allowing the solvent to evaporate.

2.1.2. Fabrication of Nanocrystal Films

Two subsets of solid-state nanorod-based thin-film samples were assembled onto silicon substrates (for XRD measurements of as-synthesized nanorods) and onto glass slides (for XRD measurements of nanorods subject to thermal sintering, and for all Raman measurements), starting from suitably formulated TiO_2-based pastes that were prepared by optimizing a previously developed method.[31] Briefly, nanocrystal suspensions in toluene, containing TiO_2 nanorods and ethylcellulose in suitable proportions, were stirred at 60 °C for 6 h. Then, terpineol was added to the mixture and stirring was continued for an additional 1 h. Toluene was finally removed by a rotary evaporator, leading to screen-printable pastes.[9, 10, 34, 49] The weight percentage composition of the pastes was: 12% TiO_2; 5% ethylcellulose; 68% terpineol; 15% organic capping.

Films based on nanorods carrying their native surfactant capping intact were prepared by depositing corresponding TiO_2 pastes onto the desired substrate, and then applying vacuum for about 7 h to remove the solvents (sample series denoted as C-AR4, C-AR8 and C-AR16, respectively).

All-inorganic films made of bare (i.e., organic-free) nanorods (samples denoted as B-AR4, B-AR8 and B-AR16, respectively) were generated by screen-printing the TiO_2 pastes onto the target substrates by the doctor-blade technique, and then annealing them at 480 °C under air for 6 h, as detailed elsehere.[9, 10, 34, 49] The conditions of the thermal cycling applied guaranteed full removal of the organic components and the formation of mesoporous thin films (typically 2 to 4.5 μm thick) made of anatase nanorods interconnected through small junction points, avoiding undesired phase transition.[9, 10, 34, 39] The size-morphological features of the sintered films were investigated by scanning electron microscopy (SEM) measurements carried out on an FEI NOVAnanoSEM200 microscope.

Commercial Degussa P25 anatase (P25) TiO_2[47] samples, in the form of nearly isotropic-shaped nanocrystals (~85 nm)[33] powders (P) and sintered films thereof (S), were measured as reference materials.

2.2. Micro-Raman Measurements

Raman spectra were collected by a commercial dispersive Invia Renishaw micro-Raman system. The Invia Raman system used a He—Ne laser as excitation source at 633 nm, focused through a 50X microscope objective on the samples, placed on a glass slide on the microscope sample holder. Scattered light was collected in backscattering configuration through the objective. Rayleigh radiation and the excitation light were rejected via an edge filter (cutoff was evaluated at a Raman shift of 120 cm^{-1}). Raman scattered light was then sent to the dispersion stage, based on a single monochromator, and detected with a Peltier cooled CCD. Spectral resolution was 4 cm^{-1}. Wavenumber calibration was internally performed using the scattered signal from a silicon reference. Acquisition conditions were checked to maximize the signal without damaging or modifying the sample. The laser power deposited onto the samples was in the range of 0.2–0.4 mW, and checked to be insufficient to drive phase transition from anatase to rutile.[18] No baseline subtraction was performed. A small amount of background luminescence, typical for the nanocrystals embedded in organic environments, was detected in the case of the surfactant-coated samples. In such circumstances, rescaling of the spectra was performed for the sake of clarity.

2.3. X-Ray Diffraction (XRD)

XRD measurements were performed with a Bruker D8 Discover diffractometer, equipped with a Cu source, a Goebel mirror, an Eurelian cradle goniometer, and a scintillator detector. XRD patterns were collected in coupled sample-detector scan mode ($\theta/2\theta$).

The XRD patterns were analyzed by using the whole-profile Rietveld-based fitting program FULLPROF,[32] according to the following procedure.[10] In the first step, the instrumental resolution function (IRF) was evaluated by fitting the XRD pattern of a LaB_6 NIST standard recorded under the same experimental conditions as those used for measuring the samples (the IRF data file was provided separately to the program to allow subsequent refinement of the XRD patterns of the samples). In the second step, the phase composition was checked by fitting the XRD patterns to the crystal structure models of different TiO_2 polymorphs and mixtures thereof. The crystalline structure of all samples was found to be safely interpretable as tetragonal TiO_2 anatase (space group $I4_1/amd$; cell parameters: $a = b = 3.7835430$ Å and $c = 9.614647$ Å; $\alpha = \beta = \gamma = 90°$). Finally, in the third step, the inhomogeneous peak broadening of the anatase TiO_2 reflections was described by a phenomenological model based on a modified Scherrer formula:

$$\beta_{h,k,l} = \frac{\lambda}{D_{h,k,l}\cos\theta} = \frac{\lambda}{\cos\theta}\sum_{\text{imp}} Y_{\text{imp}}(\Theta_h, \Phi_h) \qquad (1)$$

where $\beta_{h,k,l}$ is the size contribution to the integral width of the (h, k, l) reflection, Y_{imp} are the real spherical harmonics that were normalized according to a procedure described elsewhere.[33] The program allowed estimating the apparent coherent crystalline domain size, D_{hkl} (i.e., the size of crystallite domains that scatter X-rays coherently) along each reciprocal lattice vector (h, k, l) direction. Other refinable parameters were the unit-cell parameters. The background was unrefined and linearly interpolated. The quality of the obtained fits was checked by means of a goodness-of-fit statistical indicator (GoF). GoF values of >3–4 were considered to be satisfactory. The satisfactory fit quality and the low GoF indexes proved that the initial assumptions were correct.

3. RESULTS AND DISCUSSION

Among the various synthetic approaches employed to produce TiO_2 nanostructures, wet-chemical routes notoriously allow for the highest control over size, shape and crystal phase. These routes are essentially based on the high-temperature reaction of selected molecular precursor species in a coordinating mixture of solvent(s) and suitable ligands/surfactants.[8] The latter play several fundamental roles during the synthesis stage: they modulate the degree of the solution supersaturation by forming complexes with the precursors, tune their reactivity and govern the lattice development of the growing nanocrystals by dynamically adhering to selected crystal facets. Moreover, ligands/surfactants guarantee kinetic stabilization of the nanocrystals against undesired irreversible coalescence phenomena, by providing the surface with a robust organic molecule monolayer that ensures solubility in liquid media and enables post-synthesis processing.[8–10] Thus, whenever required, removal of such surface capping species may be performed post-synthesis either by thermal or chemical treatments.[29] The effectiveness of surface cleaning processes is usually probed by monitoring the evolution of

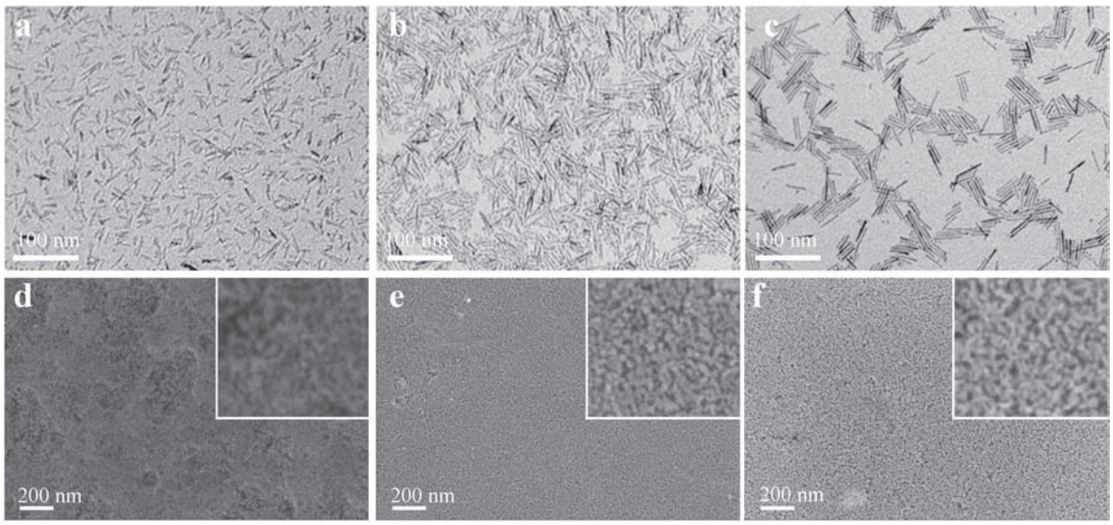

Fig. 1. (a)–(c) TEM images of the as-synthesized organic-capped anatase nanorods characterized by mean aspect ratio of 4 (a), 8 (b) and 16 (c), respectively (samples AR4, AR8 and AR16). (d)–(f) SEM images of the corresponding thermally sintered, organic-free thin films (the respective insets report 4-fold magnified images of representative areas of the films).

the characteristic vibrations of organic moieties by FTIR spectroscopy in the 4000–400 cm^{-1} range.[8] Differently, concomitant shifts of the low-frequency lattice vibrational modes in Raman spectra, which are commonly acquired in the 100–800 cm^{-1} spectral window, may provide complementary, albeit indirect, information on the nanocrystals, reflecting subtle changes in their surface chemistry and structure (see discussion in the next paragraphs). The individual effects of such alterations on Raman spectra are, normally, difficult to decouple unambiguously.

In the present study, we have comparatively examined the Raman-active lattice vibrations of anatase TiO_2 thin films assembled from wet-chemically synthesized, organic-capped anatase nanorods with different mean AR (~4, ~8 and ~16), embedded in a ethylcellulose/terpineol matrix (samples C-AR4, C-AR8 and C-AR16), and of corresponding thermally sintered (organic-free) nanorod thin films (samples B-AR4, B-AR8 and B-AR16).

Established colloidal surfactant-assisted routes[29,30] were exploited to synthesize anisotropically shaped TiO_2 nanocrystals featured by a preferential [001] lattice growth direction and tunable mean AR, all of which were surface-capped with a hydrophobic monolayer shell of oleate anion ligands. Representative TEM images of the as-prepared nanocrystals, prior to their assembly into films, are shown in Figures 1(a)–(c). The nanorods exhibited linear-shaped profiles, characterized by monodisperse short-axis (diameter) size of about 3.5 nm and mean longer-axis size (length) tunable from ~12 to ~50 nm, with relatively broader size distribution (Table I). SEM pictures of corresponding nanorod thin films obtained after thermal sintering and elimination of the organic components are reported in Figures 1(d)–(f), respectively. The SEM inspection disclosed the formation of films characterized by regular texture without any noticeable aggregates or cracks over areas of several square micrometers. The films entailed a continuous spongy network of distinguishable interconnected nanoscale building units, whose dimensional and morphological features resembled those of the starting nanocrystals. These pieces of evidences indicated that the original nanorods had been safely processed into organic-free all-inorganic mesoporous films with substantially unaltered size and morphological features.[9,10,49]

Figure 2 reports the Raman spectra of the samples, acquired over a broader spectral window (from 100 t to 3000 cm^{-1}). The as-synthesized surfactant-capped nanorods embedded in ethyl cellulose (C-AR4, C-AR8 and C-AR16) showed narrow, intense signals at ~2920–50 cm^{-1}, which authenticated the C—H stretching vibrations of the alkyl chains of oleate anions (bound to the TiO_2 surface) and of other organic matrix components. The absence of such bands in the spectra of the sintered nanorod films (B-AR4, B-AR8 and B-AR16) confirmed that all organic species had been efficiently removed upon oxidative thermal annealing. In the 200–800 cm^{-1} range all samples exhibited the fingerprint vibrational pattern of anatase TiO_2 with six normal modes.[17] Anatase has tetragonal symmetry described by the space group $I4_1/amd$.[19] The primitive cell contains two molecular units of TiO_2.[17] On the basis of factor group analysis, the six Raman active

Table I. TEM-estimated size features of the as-prepared surfactant-capped nanorods.

	AR16 [nm]	AR8 [nm]	AR4 [nm]
Longer axis	$\sim 50 \pm 8$	$\sim 35 \pm 5$	$\sim 12 \pm 2$
Shorter axis	$\sim 3.5 \pm 0.5$	$\sim 3.5 \pm 0.5$	$\sim 3.5 \pm 0.5$

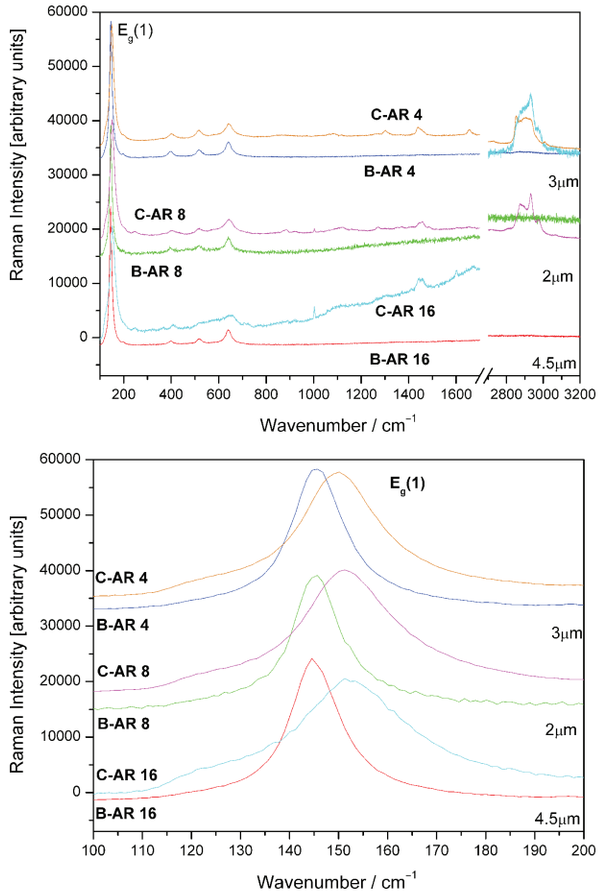

Fig. 2. Extended Raman spectra (top panel) of thin-film samples of surfactant-coated nanorods in ethylcellulose (C-AR4, C-AR8, C-AR16) and corresponding bare (i.e., organic-free) nanorods obtained upon thermal annealing of the former (B-AR4, B-AR8, B-AR16). The mean thicknesses of the films are indicated on the right side of the spectra for the respective cases. Bottom panel: detail of the $E_g(1)$ band.

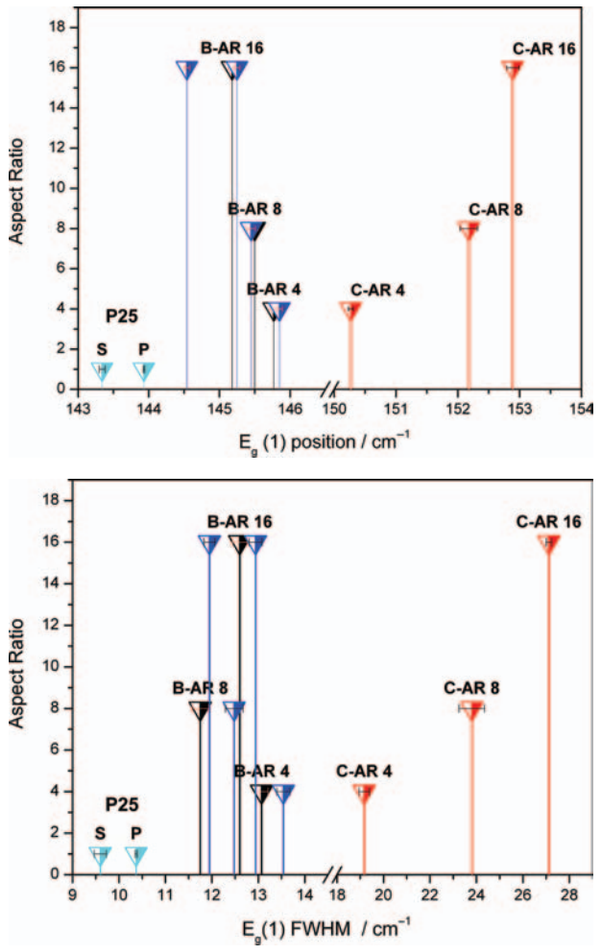

Fig. 3. Plot of the nanorod AR versus the wavenumber position (top panel) or FWHM (bottom) of the $E_g(1)$ peak, for samples of surfactant-coated nanorods (C-AR4, C-AR8, C-AR16) and organic-free sintered films thereof (B-AR4, B-AR8, B-AR16). Corresponding data for samples based on commercial TiO_2 P25-based sintered films (S) and unsintered powders (P) are reported as references. Multiple values of wavenumbers and FWHM correspond to data collected from different areas of the same sample.

normal modes were labelled according to the irreducible representation $\Gamma(i)$ (with i being an integer number) as $E_g(1)$ (at ~144 cm^{-1}), $E_g(2)$ (at 197 cm^{-1}), $B_{1g}(1)$ (at 400 cm^{-1}), $A_{1g}(1)$ and $B_{1g}(2)$ (at 520 cm^{-1}), and $E_g(3)$ (at 640 cm^{-1}), respectively.[17] In our samples, other possible phases, such as rutile and brookite, were not detected (Fig. 2), in agreement with the results of other characterization techniques documented previously.[9, 10, 29, 30]

The wavenumber position and full width at half maximum (FWHM) of the $E_g(1)$ mode in the spectra were extracted upon fitting the peaks to Lorentzian lineshapes. The plots in Figure 3 highlight the correlation holding between the AR of the pristine nanorods and the extracted values of Raman shifts and FWHMs. The Raman shift of $E_g(1)$ for the P25 reference (P) was located at 143.9 cm^{-1} , which matched with the value of 144 cm^{-1} commonly reported for bulk anatase[17] (smaller values down to 142 cm^{-1} may be also found in the literature[20]). In the spectrum of the corresponding sintered Degussa P25 nanocrystals (S), the $E_g(1)$ peak was red-shifted by about 0.5 cm^{-1} (note that the low mass fraction of rutile in P25 did not affect the $E_g(1)$ signal of anatase). The extended Raman spectrum of the powders in the region 1200–2000 cm^{-1} (data not shown) revealed negligible levels of organic contamination.

In the case of the sintered nanorod films (B-AR16, B-AR8, B-AR4—see low energy side of top panel in Fig. 3), the $E_g(1)$ peak was appeared to have increasingly blue-shifted from 144 cm^{-1} by about 1 to 2 cm^{-1} with decreasing nanorod AR (hence, volume). The corresponding variations of FWHM for $E_g(1)$ followed a similar trend as a function of AR (bottom panel in Fig. 3(b)). These findings were qualitatively in line with the size dependence of the Raman shift position and FWHM commonly reported for spherical anatase nanocrystals.[19–26]

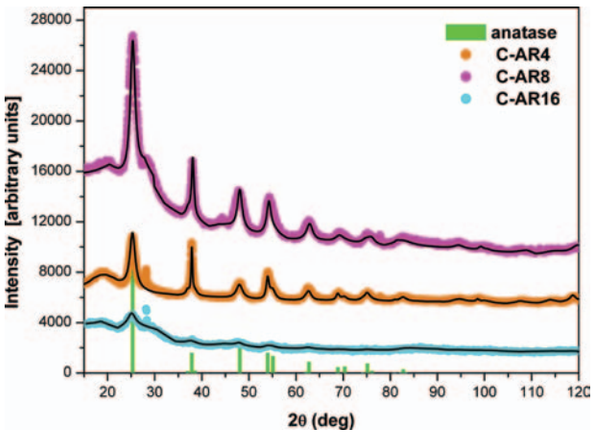

Fig. 4. Experimental XRD patterns (colored dotted lines) of samples C-AR4, C-AR8, C-AR16 (deposited on silicon) along with the corresponding Rietveld-based fits (continuous black lines). Data are rescaled for comparison purposes.

Conversely, films of the as-synthesized surfactant-coated nanorods (C-AR4, C-AR8, C-AR16-see high energy side in top panel in Fig. 3) were distinguished by much larger blue shifts of ~5 to ~10 cm^{-1}, the extent of which increased as the nanorod AR increased. The FWHM varied in the same direction (bottom panel in Fig. 3(b)).

The organic capping layer of the as-prepared nanorods (i.e., before their sintering into mesostructured films upon thermal annealing) was composed of monocarboxylic acid surfactants, namely 1-nonanoaic acid for AR4, and oleic acid for AR8 and AR16, respectively. The unsintered thin films (C-AR16, C-AR8, C-AR4) studied by us were deposited from mixtures of the freshly synthesized nanorods dispersed in ethylcellulose; therefore, the organic component should be regarded as being made of the original shell of capping surfactant agents (in the form of deprotonate anion ligands directly bound via their carboxylate moieties to the TiO_2 surface) that enwrapped ethylcellulose molecules.

The surface facets of nanocrystals can be considered as active boundaries, since their atomic configurations in vacuum (where surface is relaxed with respect to bulk structure) and in a medium (where surface may be reconstructed) are different. The Raman frequency of the low-energy $E_g(1)$ mode can be taken as a marker of interatomic potential/atomic positions in the crystal.[17]

In former studies by Oshaka et al.[17] the $E_g(1)$ mode of bulk anatase was assigned to a O—Ti—O bending-type vibration. Figure 5 displays a sketch of the anatase unit cell, where relevant crystallographic planes are highlighted. The figure clarifies that $E_g(1)$ mode relates to the bending of (6)O—Ti(1)—O(5) and (6_1)O—Ti(1)—O(5_1) bonds. In addition, it may be visualized that the (101) planes intersect the Ti(1)—O(6) bonds, which is a detail relevant to the present study (see below). Actually, the colloidal anatase nanorods investigated by us are nanostructures elongated in the [001] direction, enclosed

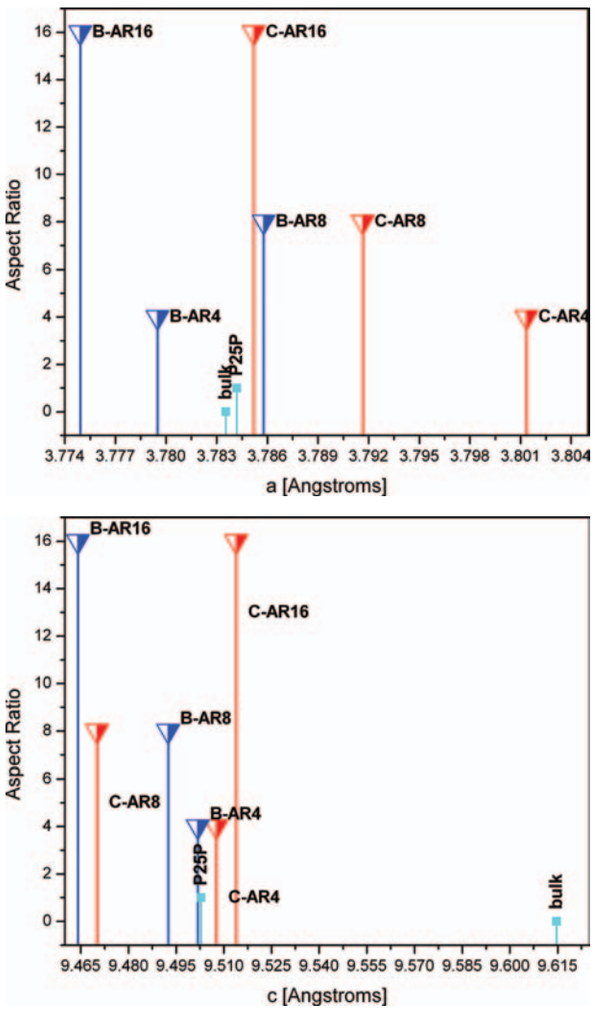

Fig. 5. Plot of the estimated unit-cell parameters $a = b$ (top panel) and c (bottom panel) versus the nanorod AR. Corresponding data for samples based on commercial TiO_2 P25 based sintered films (S) and unsintered powders (P) are reported as references.

by minor (00±1) facets at their opposite apexes and by stepped longitudinal sidewalls composed of a majority of equivalent (101)/(011) facets, as demonstrated by detailed XRD and high-resolution TEM investigations in previous works.[10, 29, 30]

According to Oshaka et al.[17] based on the G-F method,[17, 35] the low force constant of $E_g(1)$ denotes weak interaction between the two oxygens O(6) and O(5) or O(6_1) and O(5_1). The wavenumber of the normal mode is proportional to the relevant force constant, which depends on the equilibrium interatomic potential (thus, on atomic positions at equilibrium in bulk anatase). A recent experimental study on anatase substituted with O isotopes, supported by *ab initio* calculations, has demonstrated that the motion of the O atoms does not influence the $E_g(1)$ mode, whereas the motion of Ti atoms does make an impact.[48] It follows that $E_g(1)$ mode should not be associated with a O—Ti—O bending vibration, in contrast to what had been

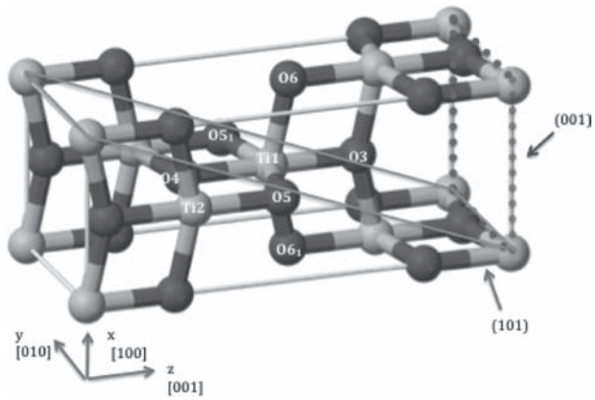

Fig. 6. Sketch of the anatase unit-cell structure. The (001) and (101) planes are marked for the sake of clarity. Atoms involved in $E_g(1)$ bending mode are labelled according to Ohsaka et al.[17]

proposed earlier.[17] However, regardless, the distribution and extension of (010) facets that are dominantly exposed on the longitudinal surfaces of the nanorods (Fig. 5) could affect the electron density around Ti atoms. Consequently, the $E_g(1)$ position can be expected to depend on the actual nanorod AR and volume, albeit to an extent that cannot be precisely predicted on the basis of current knowledge.

In the literature the blue shift of $E_g(1)$ has been commonly interpreted as arising from compressive stress, most frequently associated with a contraction of the unit cell imposed by rearrangement of surface atoms into lowest-energy configurations.[27, 28, 36, 46] Experiments reported by Xu et al.[46] on spherical 8 nm anatase nanocrystals demonstrated that the $E_g(1)$ mode could be strongly affected by the type of surface ligands. The $E_g(1)$ blue shifted by ~6 or ~9 cm^{-1} depending on whether stearic acid or dodecylbenzenesulfonic was attached to the surface, respectively. Since the application of the phonon-confinement models failed to account for the shift and width of the $E_g(1)$ band, the authors postulated a surfactant-driven compressive stress responsible for the observed Raman features, however, without providing any direct proof in favour of their hyphothesis.[46]

To assess the presence of lattice strain within the samples, especially in those made from surfactant-coated nanorods, for which the $E_g(1)$ blue-shift was anomalously large, the values of the lattice parameters were extracted by fitting the relevant XRD patterns via a Rietveld-based full-profile approach (Fig. 4).[37, 38] In Figure 5 the estimated unit-cell parameters are plotted versus the nanorod AR. For commercial P25 (made of crystalline grains with mean diameter of ~85 nm[47]) the obtained values of $a = b$ were almost coincident with those of bulk anatase ($a = b = 3.783543$ Å, $c = 9.614647$ Å), while a contraction of about 0.1 Å (1%) was found for c. Lattice distortions were assessed for all samples. In general, the unit-cell parameters decreased with decreasing nanorod volume, which agreed with the general size trend of compressive strain most frequently documented for anatase nanocrystals in this dimensional range.[25, 30, 39] Unit-cell sizes deduced for surfactant-coated nanorods were slightly larger than those estimated for their organic-free counterparts (Fig. 5), somewhat in contrast with the expectation that thermal annealing should instead alleviate the overall strain.[10] The differences in the estimated c values for bare and surfactant-coated nanorods were on the order of $5 \cdot 10^{-2}$ Å, whereas a value tended to approach that of the P25 reference, with deviations being, in fact, smaller than $2 \cdot 10^{-2}$ Å. As a matter of fact, from the data in Figure 5 it clearly emerged that by no way could the relative degree of compressive lattice strain in the samples justify, even on a qualitative basis, the variation of $E_g(1)$ energy position as a function of the nanorod size. In fact, if strain were the main responsible for the extent and direction of $E_g(1)$ shifts, then the large increase of the $E_g(1)$ frequency by up to 10% measured for the C-AR sample series should be associated with a unit-cell contraction proportionally higher than that found for the B-AR set, in apparent contrast with the experimental evidence.

Refined techniques based on first-principles (*ab initio* modelling) calculations have been applied to study the lattice dynamics and compute the Raman spectrum of bulk anatase[40, 41] and of other TiO_2 polymorphs.[42] Such first-principles studies were aimed at delivering a firm reference for the properties of nanosized or compressed phases.[40] Density Functional Theory (DFT) calculations by different methods have provided $E_g(1)$ wavenumbers and crystallographic cell parameters (from geometry optimizations) for bulk anatase, which diverge from experimental values to a little extent (by less than 2%). Unfortunately, no "standard" crystallographic set of unit cell parameters, and a corresponding Raman spectrum thereof, are available as references for bulk anatase. On the other side, it should be considered that experimental studies reported so far have actually addressed broadly differing types of samples. For example, the crystal sample studied by Oshaka et al.[17] was slightly brown in color; the sample studied by Bettinelli et al.[41] exhibited luminescence. The relevant crystallographic data acquired on such anatase materials agree with each other within a few percentages.

A detailed analysis of Raman and XRD data indicated that the significant shifts of $E_g(1)$ mode detected for the surfactant-coated nanorods (C-AR series), compared to their organic-free derivatives (B-AR series), should be a signature of the joint impact of surface and inner lattice structures, which apparently differed from those featuring Several arguments and observations can be proposed to corroborate these conclusions, as detailed in the following.

Theoretical calculations by Selloni et al.[43] have shown that the exposed five- and six-fold coordinated Ti atoms (Ti5c and Ti6c), the two- and three-fold coordinated O atoms (O2c, O3c) on the relaxed anatase (101) surface can be slightly displaced from their "bulk" (i.e., equilibrium) positions. According to this study, the coordinatively

unsaturated O2c and Ti5c atoms tend to tighten their bonding to their nearest neighbours, and relax inward, by 0.06 and 0.17 Å, respectively. As opposed, O3c and Ti6c atoms relax outwards, by 0.21 and 0.11 Å, respectively. Therefore, displacements of atoms from their equilibrium sites could influence the $E_g(1)$ frequency in small colloidal particles enclosed by (101) facets, since the latter are likely to be reconstructed to accommodate strain and/or, especially, bound ligands. In light of this theoretical support, recent experimental verification of the influence of surfactants adhering to the surface of anatase nanocrystals, which had tentatively been explained in terms of ligand-induced compressive strain,[46] should be re-interpreted as a result of surface reconstruction/modification induced upon binding of capping agents.

As to the present case, infrared spectroscopy measurements have suggested that the oleate anions attached to the surface of the as-synthesized nanorods (C-AR series) most favourably adopt a chelating bidentate binding configuration.[30] This finding agrees with theoretical studies by Selloni et al.[43] on the adsorption of formic acid (the smallest carboxylic acid molecule) on anatase (101) surfaces, which have shown that the coordination of carboxylate anions may be either monodentate or bidentate (either chelating- or bridging-type), depending on the surface density of Ti5c acid sites.[43] In addition, it is useful to recall that the preparation of the C-AR samples for Ramam analysis involved mixing the as-synthesized oleate-capped nanorods with ethylcellulose, which could thereby bind to undercoordinated free sites on their surface, and/or intercalate within the pre-existing oleate capping ligands. Under such circumstances atomic positions and bond lengths at the surface could thus be driven to rearrange further. As a consequence, significantly different $E_g(1)$ frequencies should be detected for the C-AR and B-AR nanorod sets due to their dissimilar surface features. Our experimental data were indeed consistent with such expectation. The ultimate impact of surface functionalization with organic molecules could be reasonably presumed to be proportionally more accentuated in the shorter nanorods that were indeed characterized by a larger surface-to-volume ratio.

As another important piece of evidence on the C-AR samples (Fig. 3; cf. Tables I and II) the coherent crystalline domain sizes, D_{hkl} (along the different crystallographic directions) inferred from XRD analysis diverged considerably from the corresponding sizes estimated from TEM. Note that a limited length of structural coherence is not an uncommon occurrence for colloidal nanocrystals.[53, 54] The largest size discrepancy was found between the TEM-determined length of the nanorods, and the coherent crystal size D_{001} estimated along the [001], to an extent that increased for the nanorods characterized by proportionally longer AR. Unfortunately, the XRD apparent sizes of the bare nanorods (B-AR Series) could not be extracted accurately because of the strong background interference from the glass substrate over which the nanorods were accommodated. Nevertheless, since the overall degree of crystallinity and, in turn, the size of the coherent crystalline domains are known to increase remarkably upon thermal treatment,[10] the differences between D_{001} and the TEM-measured nanorod length should be expected to be far less accentuated for the B-AR samples (relative to those assessed for their C-AR parents), to the point of vanishing in nanorods with shorter AR. In such cases, the observation that the $E_g(1)$ band blue-shifted to a gradually larger (albeit overall minor) degree with increasing nanorod volume qualitatively matched with the predictions of phonon-confinement models applied to nearly spherical (organic-unpassivated) anatase nanocrystals.[19–23, 44] In view of the results of our study, we presume that the previously identified correlation between the $E_g(1)$ frequency and the XRD-determined size held valid for samples for which the coherent crystal domain dimensions (i.e., "effective" size) essentially coincided to the TEM-measured dimensions.[19–26] Accordingly, surface-induced compressive strain could be regarded as being generally less influential, in contrast to what has been assumed so far.[44, 45]

Table II. Average coherent crystalline domain sizes, D_{hkl}, along the most relevamt crystallographic [*hkl*] directions, estimated for the as-synthesized surfactant-capped nanorods, by Rietveld analysis of the corresponding XRD patterns. Note that the (004) reflection corresponds to the lattice growth direction (i.e., along the longest axis) of the nanorod, while the (200) reflection correlates with the size of the nanorods diameter (i.e., short axis).

	C-AR16 [nm]	C-AR8 [nm]	C-AR4 [nm]
D_{101}	3.3 ± 0.5	3.1 ± 0.5	4.2 ± 0.5
D_{103}	3.3 ± 0.5	3.2 ± 0.5	6.0 ± 0.5
D_{004}	3.3 ± 0.5	7.2 ± 0.5	20.1 ± 0.5
D_{112}	3.3 ± 0.5	2.9 ± 0.5	5.5 ± 0.5
D_{200}	3.3 ± 0.5	3.4 ± 0.5	4.0 ± 0.5

On the other side, the opposite trend found for the C-AR samples, according to which the anomalously large $E_g(1)$ blue-shifts accentuated as the nanorod volume decreased, highlighted two important sources of $E_g(1)$ frequency modification: first, the nanocrystal surface structure, determined by the type of atom arrangement thereon in relation to eventual bound ligands, which should contribute to an extent proportional by the overall surface-to-volume ratio; second, the effective crystal domain size of the nanocrystals, which can be expected to diverge from TEM-determined size at relatively larger sizes and/or for nanocrystals synthesized under mild temperature conditions that may not favour complete crystallization and defect annealing.

4. CONCLUSIONS

In this work the energy shift of the $E_g(1)$ mode in the Raman spectra of anisotropic-shaped anatase TiO_2

nanocrystals has been studied in relation to their crystalline habit, structural quality and surface features. Careful examination of the Raman spectra, complemented by detailed XRD analyses, clearly indicated that the frequency of the $E_g(1)$ mode can be affected by two main types of effects: a "surface" effect, related to the atomic structure of the exposed facets and their functionalization status; a "bulk" effect, correlated with an induced "effective" size (i.e., the coherent crystalline domain size, dictated by the synthesis conditions and sample processing), a structural parameter that has never been explicitly considered in the interpretation of the Raman features of colloidal nanoparticles. On the other hand, surface-induced compressive strain may be considered as being less influential in determining the ultimate $E_g(1)$ frequency. Although it remains difficult to decouple the individual contributions from the "surface" and the "bulk" effects, our results highlight that that TEM-determined size parameters may not be straightforwardly put in relation with the Raman features, particularly when organic-coated nanocrystals generated by low-temperature synthetic routes are concerned.

Acknowledgments: The authors are grateful to Dr. M. Manca for providing sintered TiO_2 samples, and to Dr. L. Martiradonna, Professor G. Scoles and Professor A. Selloni for helpful discussion. Rocco Lassandro is acknowledged for technical support in XRD measurements.

References and Notes

1. A. L. Linsebigler, G. Lu, and J. T. Yates, *Chem. Rev*. 95, 735 (**1995**).
2. U. Diebold, G. Ruzycki, S. Hermanb, and A. Selloni, *Catal. Tod.* 85, 93 (**2003**).
3. X. Gong and A. Selloni, *J. Catal.* 249, 134 (**2007**).
4. C. Sun, L.-M. Liu, A. Selloni, G. Q. (M.) Lu, and S. C. Smith, *J. Mat. Chem.* 20, 10319 (**2010**).
5. B. O'Regan and M. Grätzel, *Nat.* 353, 737 (**1991**).
6. F. De Angelis, S. Fantacci, A. Selloni, M. Graetzel, and M. K. Nazeeruddin, *Nano Lett.* 7, 3189 (**2007**).
7. A. Hagfeldt, G. Boschloo, L. Sun, L. Kloo, and H. Pettersson, *Chem. Rev.* 110, 6595 (**2010**).
8. X. Chen and S. S. Mao, *Chem. Rev.* 107, 2891 (**2007**).
9. L. De Marco, M. Manca, R. Giannuzzi, F. Malara, G. Melcarne, G. Ciccarella, I. Zama, R. Cingolani, and G. Gigli, *J. Phys. Chem C* 114, 4228 (**2010**).
10. R. Buonsanti, E. Carlino, C. Giannini, D. Altamura, L. De Marco, R. Giannuzzi, M. Manca, G. Gigli, and P. D. Cozzoli, *J. Am. Chem. Soc.* 133, 19216 (**2011**).
11. H. G. Yang, C. H. Sun, S. Z. Qiao, J. Zou, G. Liu, S. C. Smith, H. M. Cheng, and G. Q. Lu, *Nat.* 453, 638 (**2008**).
12. A. Selloni, *Nat. Mat.* 7, 613 (**2008**).
13. S. Liu, J. Yu, and M. Jaroniec, *Chem. Mater.* 23, 4085 (**2011**).
14. (a) A. S. Barnard and L. A. Curtiss, *Nano Lett.* 7, 1261 (**2005**); (b) A. S. Barnard, *Rep. Progress Phys.* 73, 086502 (**2010**).
15. A. Vittadini, F. Sedona, S. Agnoli, L. Artiglia, M. Casarin, G. A. Rizzi, M. Sambi, and G. Granozzi, *Chem. Phys. Chem.* 17, 1550 (**2010**).
16. T. Mitsuhashi and O. J. Kleppa, *J. Am. Ceram. Soc.* 62, 356 (**1979**).
17. T. Ohsaka, F. Izumi, and Y. Fujiki, *J. Raman Spectr.* 7, 321 (**1978**).
18. P. P. Lottici, D. Bersani, M. Braghini, and A. Montenero, *J. Mat. Sci.* 28, 177 (**1993**).
19. D. Bersani, P. P. Lottici, and D. Xing-Zhao, *Appl. Phys. Lett.* 72, 73 (**1997**).
20. S. Kelly, F. H. Pollak, and M. Tomkiewicz, *J. Phys. Chem. B* 101, 2730 (**1997**).
21. A. Li Bassi, D. Cattaneo, V. Russo, C. E. Bottani, E. Barborini, T. Mazza, P. Piseri, P. Milani, F. O. Ernst, K. Wegner, and S. E. Pratsinis, *J. Appl. Phys.* 98, 074305 (**2005**).
22. W. F. Zhang, Y. L. He, M. S. Zhang, Z. Yin, and Q. Chen, *J. Phys. D: Appl. Phys.* 33, 912 (**2000**).
23. M. Ivanda, S. Musić, M. Gotić, A. Turković, A. M. Tonejcb, and O. Gamulinc, *J.. Mol. Struct.* 480–481, 641 (**1999**).
24. A. K. Arora, M. Rajalakshmi, T. R. Ravidran, and V. Sivasubramanian, *J. Raman Spectr.* 38, 604 (**2007**).
25. V. Swamy, D. Menzies, B. C. Muddle, A. Kuznetsov, L. Dubrovinsky, Q. Dai, and V. Dmitriev, *Appl. Phys. Lett.* 88, 243103 (**2006**).
26. T. P. Martin and L. Genzel, *Phys. Rev. B* 8, 1630 (**1973**).
27. C. Lejon and L. Osterlund, *J. Raman Spect.* 42, 2026 (**2011**).
28. X. J. Liu, L. K. Pan, Z. Sun, Y. M. Chen, X. X. Yang, L. W. Yang, Z. F. Zhou, and C. Q. Sun, *J. Appl. Phys.* 110, 044322 (**2011**).
29. J. Joo, S. G. Kwon, T. Yu, M. Cho, J. Lee, J. Yoon, and T. Hyeon, *J. Phys. Chem. B* 109, 15297 (**2005**).
30. (a) P. D. Cozzoli, A. Kornowski, and H. Weller, *J. Am. Chem. Soc.* 125, 14539 (**2003**); (b) L. De Caro, E. Carlino, G. Caputo, P. D. Cozzoli, and C. Giannini, *Nat. Nano.* 5, 360 (**2010**).
31. S. Ito, P. Chen, P. Comte, M. Khaja Nazeeruddin, P. Liska, P. Péchy, and M. Gratzel, *Prog. Photovolt: Res. Appl.* 15, 603 (**2007**).
32. FULLPROF: http://www-llb.cea.fr/fullweb.
33. M. Järvinen, *J. Appl. Cryst.* 26, 525 (**1993**).
34. G. Melcarne, L. Marco, E. Carlino, F. Martina, M. Manca, R. Cingolani, G. Gigli, and G. Ciccarella, *J. Mater. Chem.* 20, 7248 (**2010**).
35. E. B. Wilson, *J. Chem. Phys.* 9, 76 (**1941**).
36. V. Swamy, A. Kuznetsov, L. S. Dubrovinsky, A. Caruso, D. G. Shukin, and B. C. Muddle, *Phys. Rev. B* 71, 184302 (**2005**).
37. B. Palosz, E. Grzanka, S. Gierlotka, S. Stel'Makh, R. Pielaszek, W. Lojkowski, U. Bismayer, J. Neuefeind, H.-P. Weber, and W. Palosz, *Phase Transit.* 76, 171 (**2003**).
38. D. Dorfs, R. Krahne, C. Giannini, A. Falqui, D. Zznchet, and L. Manna, Comprehensive Nanoscience and Technology, edited by D. L. Anrews, G. D. Scholes, and G. P. Wiederrecht, Elsevier (**2011**), Vol. 1, pp. 219–270.
39. Md. Y. Ahmad and S. S. Bhattacharya, *Appl. Phys. Lett.* 95, 191906 (**2009**).
40. M. Mikami, S. Nakamura, O. Kitao, and H. Arakawa, *Phys. Rev. B* 66, 155213 (**2002**).
41. M. Giarola, A. Sanson, F. Monti, G. Mariotto, M. Bettinelli, A. Speghini, and G. Saviulo, *Phys. Rev. B* 81, 174305 (**2010**).
42. Z.-G. Mei, Y. Wang, S.-L. Shang, and Z.-K. Liu, *Inorg. Chem.* 50, 6996 (**2011**).
43. A. Vittadini, A. Selloni, F. P. Rotzinger, and M. Graetzel, *J. Phys. Chem. B* 104, 1300 (**2000**).
44. Y. Iida, M. Furukawa, T. Aoki, and T. Sakai, *Appl. Spectr.* 52, 673 (**1998**).
45. B. Pasloz, E. Grzanka, S. Gierlotka, S. Stel'Makh, R. Pielaszek, W. Lojokowski, U. Bismayer, J. Neuefeind, H.-P. Weber, and W. Pasloz, *Acta Phys Pol. A* 102, 57 (**2002**).
46. C. Y. Xu, P. X. Zhang, and L. Yan, *J. Raman Spectr.* 32, 862 (**2001**).
47. T. Ohno, K. Sakurawa, K. Tokieda, and M. Matsumara, *J. Cat.* 203, 82 (**2001**).

48. O. Frank, M. Zukalova, B. Laskova, J. Kurti, J. Koltaib, and L. Kavan, *Phys. Chem. Chem. Phys.* 14, 14567 (**2012**).
49. L. De Marco, M. Manca, R. Buonsanti, R. Giannuzzi, F. Malara, P. Pareo, L. Martiradonna, N. Giancaspro, P. D. Cozzoli, and G. Gigli, *J. Mater. Chem.* 21, 13371 (**2011**).
50. H. Chang and P. J. Huang, *J. Raman Spectrosc.* 29, 97 (**1998**).
51. D. Georgescu, L. Baia, O. Ersen, M. Baia, and S. Simon, *J. Raman Spectrosc.* 43, 876 (**2012**).
52. S. K. Gupta, R. Desai, P. K. Jha, S. Sahoob, and D. Kirinc, *J. Raman Spectrosc.* 41, 350 (**2010**).
53. V. Petkov, P. D. Cozzoli, R. Buonsanti, R. Cingolani, and Y. Ren, *J. Am. Chem. Soc.* 131, 14264 (**2009**).
54. M. Levy, A. Quarta, A. Espinosa, A. Figuerola, C. Wilhelm, M. Garcia-Hernandez, A. Genovese, A. Falqui, D. Alloyeau, R. Buonsanti, P. D. Cozzoli, M. A. Garcia, F. Gazeau, and T. Pellegrino, *Chem. Mater.* 23, 4170 (**2011**).